

# Photon-number uncertainty in a superconducting transition edge sensor beyond resolved-photon-number determination

Zachary H. Levine,<sup>1,\*</sup> Boris L. Glebov,<sup>1,2</sup> Alan L. Migdall,<sup>1,2</sup> Thomas Gerrits,<sup>3</sup>  
Brice Calkins,<sup>3</sup> Adriana E. Lita,<sup>3</sup> and Sae Woo Nam<sup>3</sup>

<sup>1</sup>National Institute of Standards and Technology, Gaithersburg, Maryland 20899, USA

<sup>2</sup>Joint Quantum Institute, National Institute of Standards and Technology and University of Maryland, Gaithersburg, Maryland 20899, USA

<sup>3</sup>National Institute of Standards and Technology, Boulder, Colorado 80305, USA

\*Corresponding author: zlevine@nist.gov

Received June 20, 2014; revised July 22, 2014; accepted July 28, 2014;  
posted August 1, 2014 (Doc. ID 214380); published September 10, 2014

As part of an effort to extend fundamental single-photon measurements into the macroscopic regime, we explore how best to assign photon-number uncertainties to output waveforms of a superconducting transition edge sensor and how those assignments change over that extended dynamic range. Three methods are used. At the lowest photon numbers (up to 20 photons), the widths of histogram peaks of individual waveforms are used to determine the uncertainty. From 100 to 1000 photons, mean waveforms are used to create a photon-number scale. The photon-number uncertainty of the detector in this range is given by the excess of the total variance of the photon number obtained from individual waveforms on this scale beyond the shot noise due to the source. In the midrange (from 10 to 100 photons), including a range where the two other methods do not produce definitive results, we fit waveforms to several adjacent mean waveforms to estimate the photon-number uncertainty. A one-standard-deviation uncertainty in photon number of no more than  $\pm 1$  is found for pulses of up to 100 photons.

OCIS codes: (040.5570) Quantum detectors; (120.5630) Radiometry.

<http://dx.doi.org/10.1364/JOSAB.31.000B20>

## 1. INTRODUCTION

A goal of metrology is to link macroscopic observables to fundamental physics and to fundamental units of measurement that can be a quantum. One promising tool in pursuit of that goal [1–3] is the superconducting transition edge sensor (TES), which offers a number of remarkable photon-detection characteristics. Because it is a microcalorimeter whose thermal sensor is a superconductor operated in the transition between normal and superconducting, it can sense the heat of a single photon and even resolve, in some cases, the number of photons. In addition, because the TES works by registering the heat of absorbed radiation, its spectral sensitivity is governed just by its reflectance. With the proper coatings, a detection efficiency of 95% [4] was reported, and the use of a fiber coupling with index-matched resin led to a 98% [5] efficiency. The ability of a TES to resolve up to 23 photons [6] and 29 photons [7] has been reported. With such efficiency and number resolution, it is clear why this detector is of interest to the metrology community. There is interest in extending its operation to as large a dynamic range as possible [8,9].

An important step in this effort is to determine the uncertainty with which the output response of a TES can be turned into a measurement of the number of photons. It is particularly challenging to estimate this uncertainty in the regime between where photon numbers are easily distinguished (the few-photon regime) and the regime where the uncertainty in the detector response dominates over the shot noise of the

input light pulses (the high-photon-number regime). At intermediate light levels, the photon number may be determined to better than the shot noise of the source, but the uncertainty is larger than that of a single photon.

Our group's original work along these lines resulted in an upper bound on the uncertainty of the photon-number determination [8]. Yet there are applications where more definite knowledge of such an uncertainty would be desirable. Measuring the photon-number uncertainty of a squeezed light state or source are such applications. The metrological applications of squeezed light include Michelson [10] and Fabry–Perot [11] interferometers. Other applications measure femtowatt power levels [9,12,13]. The regime is also near the sensitivity for human vision. An early experiment measured the threshold for sensitivity of human vision using pulses of several tens to over 100 quanta of blue–green light incident on the cornea [14]. In the present work, we go beyond the previous determination of an uncertainty bound [8] and provide a definite estimate of the uncertainty.

## 2. PHOTON-NUMBER UNCERTAINTIES FOR A TRANSITION EDGE SENSOR DETECTOR

Gerrits *et al.* [8] reported the acquisition of sets of 20,480 output waveforms from a TES detector with laser pulses with 45 average values of pulse energy, for a total of 921,600 pulses. The pulse energies range from a mean  $\langle n \rangle$  of 2.0 photons per pulse to 6.4 million photons per pulse at a wavelength of

1550 nm. The large data set allowed for the estimation of uncertainties throughout most of the range. In this paper, we explore more fully the estimation of the photon-number uncertainty of the detector when that value is below the shot noise of the source.

### A. Uncertainties in the Photon-Counting Regime

Previously, the Poisson-influenced  $K$ -means algorithm (PIKA) [6] was introduced and applied to the TES data of Gerrits *et al.* [8]. The motivation was to extract the ideal response of the detector in a model-free way. A differential geometry approach has been applied to TES data with similar goals [15]. The two major assumptions behind PIKA are that more photons yield a larger response, which allows the photon responses to be ordered, and that the source obeys a Poisson distribution, which allowed the ordered responses to be clustered using a variant of the  $K$ -means clustering algorithm [16,17] governed by Poisson statistics.

PIKA assigned effective photon numbers to each detected waveform generated from laser pulses with the same average number of photons. Histograms of these effective photon numbers showed peaks at integers, extending the visibility of the peaks from 19 photons using a matched-filter method to 23 photons. (See Figs. 3 and 4 of [6].) The results for PIKA from two different mean photon numbers are shown in Fig. 1. The figure shows that as the number of photons in a pulse increases, so does the uncertainty in the number of photons detected. Here, the uncertainty is determined from the standard deviation of the peaks in the histogram that are fit to Gaussians. A consequence of the uncertainty increasing above 0.4 photons is the disappearance in the histogram peak visibility. We illustrated this effect in Fig. 2, in which we model a histogram by summing a set of Gaussians with a given standard deviation and unit spacing. The figure shows the modulation decreases as the standard deviation increases. For example, the Rayleigh criterion (typically used to see if optical point sources are barely resolved) of a trough-to-peak ratio of  $8/\pi^2$  is achieved for  $\sigma = 0.39$ . To estimate the uncertainty for a larger number of photons per pulse, a different method is required.

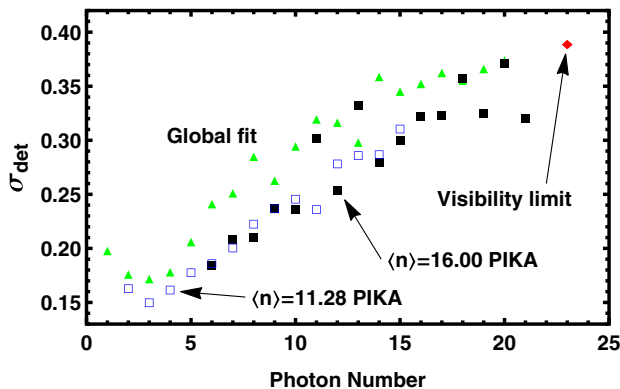


Fig. 1. Standard deviation of the Gaussian fits from PIKA: fit to waveforms with a mean photon number of 11.28 (empty blue squares), fit to waveforms with a mean photon number of 16.00 (filled black squares), from the global fit to the waveforms as described in the text (filled green triangles), and from an estimate of the end of the visibility of the fringes (filled red diamond) (from [6]) and the sum-of-Gaussian model.

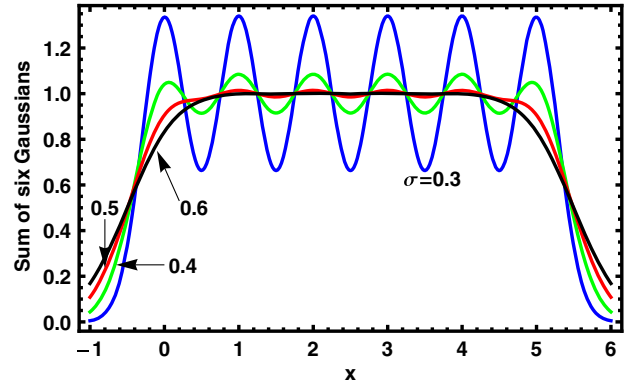


Fig. 2. Sum of six Gaussians with unit area and standard deviations  $\sigma$  given by 0.3 (blue), 0.4 (green), 0.5 (red), and 0.6 (black) centered on the integers 0–5 in the abstract variable  $x$ . The sum becomes flatter as  $\sigma$  is increased.

### B. Uncertainties Near the Shot-Noise Limit

For a set of pulses with Poisson-distributed photon numbers with a known mean  $\langle n \rangle$ , the observed variance  $\sigma_{\text{tot}}^2$  has contributions from detector noise  $\sigma_{\text{det}}^2$  and the variance of the source distribution  $\langle n \rangle$  (equal to the mean for a Poisson distribution). Assuming the detector noise is independent of  $\langle n \rangle$  for photon numbers  $n$  within a couple of standard deviations of  $\langle n \rangle$ , the variances will sum:

$$\sigma_{\text{tot}}^2 = \sigma_{\text{det}}^2 + \langle n \rangle. \quad (1)$$

For the data of [8], the mean number is known absolutely by evaluating  $\langle n \rangle$  in the photon-counting regime and noting that  $\langle n \rangle$  increases by a fixed factor as one or more attenuators are removed from the path of the beam.

Before  $\sigma_{\text{tot}}^2$  can be found for a given data set, we need to be able to assign an effective photon number  $n^{(\text{eff})}$  (not in general an integer) to each detected waveform. In [8], this was done using thermal modeling of the detector with fitting to the position of the trailing edge of the output waveforms. Here, we use PIKA to make a scale from the data.

PIKA was run on the 21 data sets with the lowest mean photon numbers, ranging in steps of a constant factor of very nearly  $\sqrt{2}$  from  $\langle n \rangle = 2.005$  to  $\langle n \rangle = 1950$ . PIKA groups the waveforms into clusters with similar responses and assigns a photon number to each cluster. The means of the waveform clusters are tentatively taken to be the response for that photon number. Previously [6], the cluster means were seen to be independent of  $\langle n \rangle$  and dependent only on  $n$ , the exact photon number, in cases examined with a few tens of photons. (In this paper, we use  $n$  to denote both the number of photons detected in a particular case and also to index the average detector response when  $n$  photons are detected.)

It is not possible to extend this matching across the present data set, because the spacing increases geometrically with  $\langle n \rangle$ , whereas the standard deviation increases only as  $\langle n \rangle^{1/2}$ . Hence in many cases, waveforms with an individual photon number are only measured once. If the uncertainty in photon number is not negligible in comparison with  $\langle n \rangle^{1/2}$ , we cannot take the  $n$  values derived from PIKA as accurate since the PIKA-derived clusters (which ideally contain the responses with exactly  $n$  detected photons) will mix detector responses from several adjacent photon numbers.

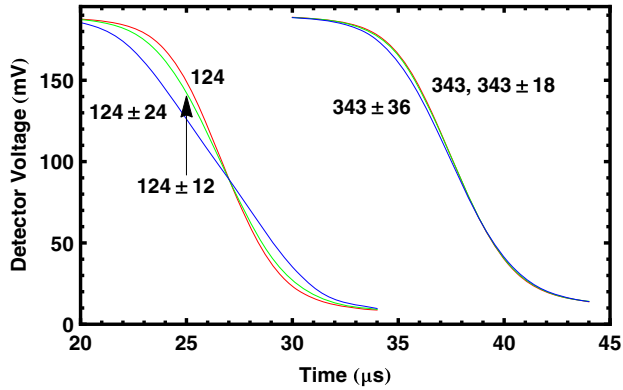


Fig. 3. Mean response waveforms of the detector for the data from the clusters with  $n = 124$  and  $\langle n \rangle = 124.7$  and  $n = 343$  and  $\langle n \rangle = 342.6$  are compared to averages of pairs of clusters as marked. (The curve for  $n = 343$  is hidden by the curve for  $n = 343 \pm 18$ .)

However, in the case  $n \approx \langle n \rangle$ , the effect of assignment uncertainty on the cluster-mean waveforms is small. Some of the waveforms contributing to the cluster-mean waveform for  $n$  photons have  $n + 1$  (or  $n + 2$  or more) photons, but these will be almost completely compensated by contributions from waveforms with  $n - 1$  (or  $n - 2$  or fewer) photons. The magnitude of the averaging effect may be seen in Fig. 3. Here, we compare the cluster-mean waveform with  $n \approx \langle n \rangle$  photons to averages of cluster means with photon numbers that average to  $\langle n \rangle$ . The amount of uncertainty introduced by including pulses from nearby photon numbers in the cluster is seen to be very small for  $n = 124$  or  $n = 343$ . The main effect is to make the slope of the trailing edge slightly less steep than it otherwise would be. Interestingly, there is a cross-over point in the middle of the trailing edge that is nearly independent of a symmetric misclassification of the photon number.

The cluster-mean waveforms are shown together in Fig. 4. The means are roughly evenly spaced in the logarithm of the photon number, with a decrease in spacing for photon numbers over a few hundred. The trailing edges for up to a couple hundred photons are seen to be similar, as reported earlier [6], although the slope decreases very slightly with a larger photon number. The purpose of Fig. 4 is to help create a global scale

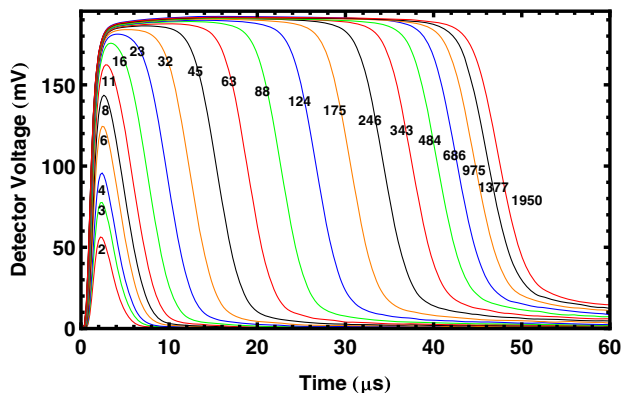


Fig. 4. Response curves for the TES detector as a function of the number of incident photons. These curves were obtained by taking the means of the waveforms obtained through PIKA, selecting the photon number  $n$  (labeled on graph) to be the nearest integer to the mean photon number  $\langle n \rangle$  for the data set. Noting that these curves never cross, we may regard this figure as a contour plot of a function  $n_{\text{scale}}(t, V)$ .

for the identification of  $n^{(\text{eff})}$  over a broad range of photon numbers.

To determine the  $\sigma_{\text{tot}}$ , we need to assign an individual effective photon number to each waveform  $V_i(t)$ , where  $V$  is the detector voltage,  $t$  is the time from the start of the pulse, and  $i$  indexes the laser pulses. We choose to do so with the following procedure. First, we determine the peak of the waveform and discard the leading edge. Next, we determine where the waveform falls below a given value  $V_{\text{low}} = +31$  mV relative to the voltage output of the quiescent detector and truncate the curve at that point. We do this so that the photon-number assignment will be independent of noise late in the waveform, which occasionally comes above threshold. Since the cluster-mean waveforms are very close together for large voltages  $V \geq V_{\text{hi}} = 153$  mV, these parts of the voltage waveforms are ignored as well. In addition, four out of 430,080 waveforms did not fall as low as  $V_{\text{low}}$  within 30  $\mu\text{s}$  and were dropped from the analysis.

Each of the remaining points  $(t, V)$  in each waveform is considered to be an independent estimate of the number of photons incident in the pulse, obtained by interpolating the functions shown in Fig. 4. The interpolation is done in the dependent variable  $\ln n_{\text{scale}}$  drawn from the cases  $n \approx \langle n \rangle$ . Because the middle of the region is best known, we form a weighted average with each point assigned a weight  $w(V) = |V - V_{\text{mid}}|$ , where  $V_{\text{mid}} = (V_{\text{hi}} + V_{\text{low}})/2$ . The function used to determine the measured photon number for a waveform  $i$  is

$$n_i^{(\text{eff})} = \exp \left[ \frac{\sum_t w(V_i(t)) \ln n_{\text{scale}}(t, V_i(t))}{\sum_t w(V_i(t))} \right], \quad (2)$$

where the discrete sum is over the times in the trailing edge, as described above.

The global scale may be compared to local scales derived by PIKA on measurements at a single mean photon number. Results are shown for the case of an average photon number of 343 in Fig. 5. The scales are seen to be in agreement to about one photon for all clusters whose photon numbers are within two standard deviations of the mean. The near-identity function suggests that the bias of our scale is small. Similar plots for lower average photon numbers show tighter

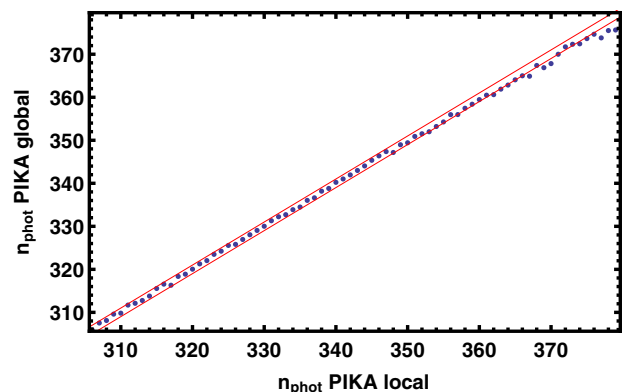


Fig. 5. Waveforms associated with the cluster means found from PIKA for the data with  $\langle n \rangle = 342.6$  (called  $n_{\text{phot}}$  PIKA local) are plotted with effective photon numbers evaluated from Eq. (2) using the global scale of Fig. 4 (called  $n_{\text{phot}}$  PIKA global). The red lines are drawn with an offset of  $\pm 1$  photon from the identity function.

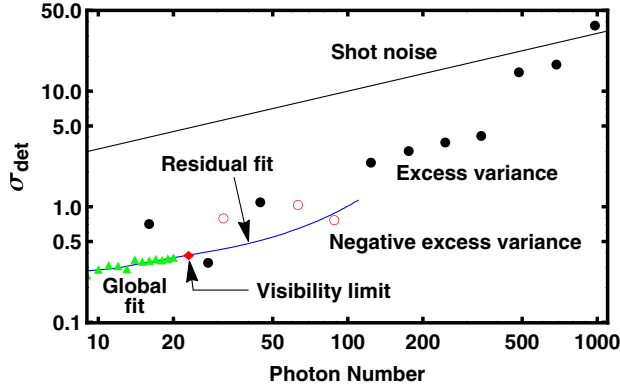


Fig. 6. Black line labeled “shot noise” is  $\sqrt{\langle n \rangle}$ . The standard deviation attributed to the detector obtained by subtracting the Poisson variance (shot noise) from the total variance then taking the square root (filled black circles when this value is real, hollow red circles when this value is imaginary, i.e., negative calculated variance). Fit assuming  $\sigma_{\text{det}}(n) \propto a^{-1/2}(n)$ , where  $a(n)$  describes the parabola of residuals [Eq. (5)], and  $n$  is the photon number (blue line). The green triangles and red diamond are described in Fig. 1.

agreement. For higher average photon numbers, the agreement deteriorates to 5 photons for the average photon number of 975.

The results for the photon-number uncertainty  $\sigma_{\text{det}}$  are shown in Fig. 6. For photon numbers just beyond where the fringe visibility disappears [6], the uncertainty values are sometimes imaginary (i.e., the calculated excess variance is negative). We attribute such out-of-range values to our inability to estimate  $\sigma_{\text{tot}}^2$  with sufficient accuracy. Since there is no physical justification for negative variance, we interpret the first six circles as representing a bound on the excess noise of approximately 1 photon. However, for the remaining seven clusters, the  $\sigma_{\text{det}}$  is an increasing function of the photon number of the pulse. As the shot-noise limit is approached, the method of subtracting the shot noise to obtain the excess variance is increasingly reliable because the process moves from the subtraction of two nearly equal numbers to the subtraction of two numbers that differ by a factor of two. The detector noise is approximately equal to the shot noise for 1000 photons, as reported previously [8].

### C. Uncertainties of a Half to a Few Photons

How can we estimate the photon-number uncertainty when it is too large for fringes to be visible in the histogram of effective photon numbers, yet too small for the excess variance method of Eq. (1) to work reliably? Our strategy is the following: (1) we fit the global scale of Fig. 4 with functions that allow us to interpolate to a fine-grained global scale; (2) we use the fine-grained global scale to estimate residuals for each waveform over several photon numbers  $n$  near the best fit; (3) we correlate a parameter from the fit to the standard deviations of the Gaussians used to fit effective photon numbers at low photon numbers with clear peaks; and finally (4) we extrapolate correlation for photon numbers past the visibility limit.

Although PIKA produces estimates of the ideal waveforms for every photon number, we were concerned that effective photon numbers estimated by PIKA could be affected by detector noise. Accordingly, we derived a set of ideal waveforms by a fit to the central mean waveforms given by PIKA, which

are shown in Fig. 4. The fitting procedure was as follows. First, we found that the differences between two cluster mean waveforms (i.e.,  $\bar{V}_n(t) - \bar{V}_{n-1}(t)$  in the notation of [6]) could be described by a sum of a lognormal distribution at short times and a Gaussian for the trailing edge. Symbolically,

$$D_n(t) = A_1(n) \exp \left[ -\left( \frac{\ln n - \mu_1(n)}{2\sigma_1(n)^2} \right)^2 \right] + A_2(n) \exp \left[ -\left( \frac{n - \mu_2(n)}{2\sigma_2(n)^2} \right)^2 \right] \quad (3)$$

for the parameters  $A_1$ ,  $\mu_1$ ,  $\sigma_1$ ,  $A_2$ ,  $\mu_2$ , and  $\sigma_2$ , which are the amplitudes, means, and standard deviations. The templates themselves were found from

$$T_n(t) = T_{n-1}(t) + D_n(t), \quad (4)$$

with  $T_0(t) = 0$ . The parameters of the difference templates varied with photon number  $n$  as  $\alpha_j \exp(-n/\tau_j) + \beta_j n + \gamma_j$ , where  $j$  can refer to any of the six parameters. Of course,  $T_n(t) \approx \bar{V}_n(t)$  for the  $\bar{V}_n(t)$  in Fig. 4, but the  $T_n(t)$  are defined for all integer photon numbers  $n$  between 1 and 1950.

We find the squared residuals  $s_i(n)$  from the templates associated with a given photon number  $n$ . We fit these residuals to a parabola,

$$s_i(n) = \frac{a_i}{2} (n - n_i^{(0)})^2 + c_i, \quad (5)$$

where  $a_i$  is the curvature,  $n_i^{(0)}$  is the effective photon number at the minimum, and  $c_i$  is a constant.

If we assume that the noise in the system causes the mean squared deviation to be independent of the number of photons, we expect  $\sigma_{\text{det}} \propto a_i^{-1/2}$ . The fact that the trailing edges of the waveforms shown in Fig. 4 have a shape that is nearly independent of the photon number for the first couple hundred photon numbers makes such a relation plausible.

Using one fitting parameter for the proportionality constant between  $\sigma_{\text{det}}$  and  $a_i^{-1/2}$ , we obtain the result shown in Fig. 6. We do not extend the fit much past 100 photons because of our reliance on the assumption that the trailing edge is independent of the photon number. The curve matches both the standard deviations from 10 photons and up, as well as the values obtained from the excess standard deviation method. The fit is not particularly good below 10 photons, but the assumption that the trailing edge is independent of photon number does not hold where the pulse height is growing toward its saturated level, as seen in Fig. 4.

## 3. SUMMARY AND CONCLUSIONS

Our goal was to estimate the photon number uncertainty for a superconducting TES in the regime in which histograms of the effective photon numbers show no peaks, but the photon-number uncertainty of the detector is less than the shot noise of the optical source.

First, we showed from a model and from data that when the photon-number uncertainty exceeds 0.4, the visibility of photon-number peaks in a histogram of effective photon numbers vanishes. The implication is that when the noise of the detector, parameterized as uncertainty in the number of photons in

the detected signal, exceeds 0.4 photons, no algorithm can find peaks in the histogram of effective photon numbers.

When the noise of the detector is a significance fraction of the shot noise, it is possible to estimate the detector noise by finding the total standard deviation of photon number and subtracting the shot noise contribution. [8] To do this, we applied the PIKA [6] to TES data with mean photon numbers up to 1950. We established a scale for the response of the detector between the limit of fringe visibility and the shot-noise-dominated regime by making the approximation that the mean of the voltage waveforms in a cluster taken from near the mean photon number of the pulses is accurately given. By exaggerating the effect of photon-number uncertainty on these mean waveforms, we showed the central waveforms were likely to have little bias. The scale for the effective photon number was chosen to have low bias, while still including enough data from each waveform to allow for a considerable amount of averaging.

The two methods left a gap in the uncertainty estimate between 20 photons and 100 photons, although the photon-number uncertainty was bounded by the excess detection method to be roughly 1 for this range. We estimate the photon-number uncertainty in the gap by noting we had empirical and theoretical reasons to believe that the photon-number uncertainty was determined by the width of a parabola formed from residuals of a given waveform versus ideal waveforms for different photon numbers [Eq. (5)].

In the end, we are able to estimate that a one-standard-deviation photon-number uncertainty of 1 or less can be achieved with up to 100 detected photons. We agree with the previous conclusion [8] that the shot noise limit is reached at 1000 photons.

We are hopeful that the methods developed herein will be useful to extend the dynamic range of metrologically important endeavors such as light source development with below-shot-noise number uncertainties and experimentation in regimes with very low light but with fluxes above the photon counting limit.

## ACKNOWLEDGMENTS

We are pleased to acknowledge discussions with Adam Pintar.

## REFERENCES

1. A. Avella, G. Brida, I. P. Degiovanni, M. Genovese, M. Gramegna, L. Lolli, E. Monticone, C. Portesi, M. Rajteri, M. L. Rastello, E. Taralli, P. Traina, and M. White, "Self consistent, absolute calibration technique for photon number resolving detectors," *Opt. Express* **19**, 23249–23257 (2011).
2. L. Lolli, G. Brida, I. P. Degiovanni, M. Gramegna, E. Monticone, F. Piacentini, C. Portesi, E. Taralli, and P. Traina, "Ti/Au TES as superconducting detector for quantum technologies," *Int. J. Quantum Inform.* **9**, 405–413 (2011).
3. F. Piacentini, E. A. Goldschmidt, M. G. Miingolia, I. P. Degiovanni, M. Gramegna, I. R. Berchera, S. V. Polyakov, S. Peters, S. Kück, E. Taralli, L. Lolli, M. Rajteri, M. G. A. Paris, A. Migdall, G. Brida, and M. Genovese, "Some recent progresses in quantum tomography realised at INRIM," *Proc. SPIE* **8875**, 88750G (2013).
4. A. E. Lita, A. J. Miller, and S. W. Nam, "Counting near-infrared single-photons with 95% efficiency," *Opt. Express* **16**, 3032–3040 (2008).
5. D. Fukuda, G. Fujii, T. Numata, K. Amemiya, A. Yoshizawa, H. Tsuchida, H. Fujino, H. Ishii, T. Itatani, S. Inoue, and T. Zama, "Titanium-based transition-edge photon number resolving detector with 98 percent detection efficiency with index-matched small-gap fiber coupling," *Opt. Express* **19**, 870–875 (2011).
6. Z. H. Levine, T. Gerrits, A. L. Migdall, D. V. Samarov, B. Calkins, A. E. Lita, and S. W. Nam, "An algorithm for finding clusters with a known distribution and its application to photon-number resolution using a superconducting transition-edge sensor," *J. Opt. Soc. Am. B* **29**, 2066–2073 (2012).
7. L. Lolli, E. Taralli, and M. Rajteri, "Ti/Au TES to discriminate single photons," *J. Low Temp. Phys.* **167**, 803–808 (2012).
8. T. Gerrits, B. Calkins, N. Tomlin, A. E. Lita, A. Migdall, S. W. Nam, and R. Mirin, "Extending single-photon optimized superconducting transition edge sensors beyond the single-photon counting regime," *Opt. Express* **20**, 23798–23810 (2012).
9. L. Lolli, E. Taralli, M. Rajteri, T. Numata, and D. Fukuda, "Characterization of optical fast transition-edge sensors with optimized fiber coupling," *IEEE Trans. Appl. Supercond.* **23**, 2100904 (2013).
10. C. M. Caves, "Quantum-mechanical noise in an interferometer," *Phys. Rev. D* **23**, 1693–1708 (1981).
11. J. A. Gifford and C. M. Savage, "Quantum theory of interferometric length measurement with inefficient photodetectors," *Phys. Rev. A* **43**, 1484–1491 (1991).
12. H. Lo, P. Su, Y. Cheng, P. Wu, and Y. Chen, "Femtowatt-light-level phase measurement of slow light pulses via beat-note interferometer," *Opt. Express* **18**, 18498–18505 (2010).
13. B. S. Karasik and R. Cantor, "Demonstration of high optical sensitivity in far-infrared hot-electron bolometer," *Appl. Phys. Lett.* **98**, 193503 (2011).
14. S. Hecht, S. Schlear, and M. H. Pirenne, "Energy at the threshold of vision," *Science* **93**, 585–587 (1941).
15. D. J. Fixsen, S. H. Moseley, T. Gerrits, A. E. Lita, and S. W. Nam, "Optimal energy measurements in nonlinear systems: an application of differential geometry," *J. Low Temp. Phys.* **176**, 16–26 (2014).
16. G. Hamerly and C. Elkan, "Alternatives to the  $k$ -means algorithm that find better clusterings," in *Proceedings of the 11th International Conference on Information and Knowledge Management* (Association for Computing Machinery, 2002), pp. 600–607.
17. C. Ding and X. He, " $K$ -means clustering via principal component analysis," in *Proceedings of the 21st International Conference on Machine Learning* (Association for Computing Machinery, 2004), pp. 29–37.